

THE R.M. SANTILLI FOUNDATION

PROMOTING BASIC SCIENTIFIC ADVANCES AND SCIENTIFIC ETHICS

Preliminary and partial version
July 1, 2012

SCIENTIFIC DESCRIPTION OF
SANTILLI'S COMPARITIVE TEST
OF THE GRAVITY OF ELECTRONS AND POSITRONS
IN A HORIZONTAL SUPER-COOLED VACUUM TUBE

The R. M. Santilli Foundation
150 Rainville Rd
Tarpon SDprings, FL 34689
board@santilli-foundation.org
Tel. 727-688 3992

BonPhysics Research and Investigations BV; Laan van Heemstede 38, 3297AJ Puttershoek, The Netherlands, T: +31(0)78 6767023, E: victor@bonphysics.nl, W: www.bonphysics.nl

The R. M. Santilli Foundation; 35246 US 19 North Suite 215; Palm Harbor, FL 34684, U.S.A.

Preface

This report is made exclusively for use by the R. M. Santilli Foundation. It describes the feasibility of the technical realization of an experiment first proposed by R. M. Santilli in 1994. It includes a first planning and budget for a complete instrument to perform the scientific experiment.

This experiment can decisively give an answer to the question “Do electrons and positrons get both attracted by Earth’s gravitation or has the gravity force opposite sign for electrons and positrons?”

The contents of this report was generated by BonPhysics for the R. M. Santilli Foundation by means of

resources of BonPhysics,
information obtained from the R. M. Santilli Foundation,
information obtained from Delft University of Technology,
references as quoted in the reference list.

Contents

<u>Preface</u>	2
<u>Contents</u>	3
<u>1. Introduction</u>	4
<u>2. Principle of Santilli's proposal</u>	7
<u>2.1. Physics</u>	7
<u>2.2. Measurements</u>	8
<u>3. Equipment</u>	10
<u>3.1. Electron and positron sources</u>	11
<u>3.2. Shielded vacuum tube</u>	11
<u>3.2.1. Tube length</u>	11
<u>3.2.2. Super-cooled shielding</u>	12
<u>3.2.3. Shielding inner-surface condition</u>	13
<u>3.2.4. Vacuum</u>	13
<u>3.2.5. Lens system</u>	14
<u>3.2.6. Magnetic guide field</u>	14
<u>3.2.7. Magnetic field compensation</u>	15
<u>3.2.8. Rotation around beam axis</u>	15
<u>3.3. Detection</u>	16
<u>3.4. Infrastructure</u>	16
<u>4. Time schedule</u>	17
<u>5. Budget</u>	18
<u>6. Existing suitable facilities</u>	20
<u>References</u>	21
<u>Summary</u>	23
<u>Appendix A: Gravity aberration of a perfect particle lens</u>	24
<u>Appendix B: Surface patch potential effect</u>	27
<u>Appendix C: Gravity deflection measurement procedure</u>	29
<u>Appendix D: Decisive outcome</u>	32
<u>Appendix E: Optimal size</u>	34
<u>Appendix F: Influence of Sun and Moon</u>	36

1. Introduction

Sir Isaac Newton writes in the last chapter of his Principia [1]: "But hitherto I have not been able to discover the cause of gravity from phenomena, and I frame no hypothesis; for whatever is not deduced from the phenomena is to be called an hypothesis; and hypotheses, whether metaphysical or physical, whether of occult qualities or mechanical, have no place in experimental philosophy ". According to Newton only experiment scan teach us more about the cause of gravity. Gravity experiments with neutral mass, however, are not decisive for the outcome of gravity experiments on (charged) elementary particles or on antimatter. It is therefore of the utmost importance that experiments are performed to measure the gravitational mass of charged elementary particles and antiparticles.

Since the science revolution at the beginning of the 20th century our worldview is based on quantum mechanics and relativity. One of the principles of the general theory of relativity is the equivalence principle [2], according to which the gravitational mass and inertial mass of all objects is exactly the same. The current developments in Cosmology show that under this principle there should be so-called 'dark matter' and 'dark energy', otherwise some measurements can not be explained [3,4]. The equivalence principle is a basis for our interpretation of reality and it determines the way we search for new solutions to our current technical limitations. Such as the search for new clean energy sources. It is therefore very important that the experimental basis of the principle is as broad as possible.

To date, no experiment, on Earth or in space, can negate this principle. It is measured accurately for macroscopic objects [5,6] and for neutral neutrons [7,8,9]. Nevertheless, one can imagine that gravity acts different on bosons or fermions [10], charged or uncharged elementary particles or on matter and antimatter [11]. At CERN [12,13] and Fermilab [14,15] efforts are underway to test the equivalence principle for neutral antimatter where problems with electric and magnetic stray fields are avoided.

According to Einstein, it is conceivable that the equivalence principle does not hold for charged particles or antiparticles [16]. This is supported by Santilli with the development of the isodual theory of antimatter [17]. These suggestions lack experimental verification. Even the gravitational mass of the electron is not measured. Although already in the 1960's an attempt was made by Witteborn and Fairbank [18]. The purpose of this experiment was to measure the gravity on electrons and positrons. However, it was only performed with electrons and the result is disputed in literature. The electrons in the performed experiment fell only with a maximum of 10 % of the gravitational acceleration. The experiment was not repeated with positrons because of the lack of an adequate positron source [19].

Already in 1994 Santilli [20,21] proposed an experiment to measure the gravity on particles and antiparticles. The novelty was that use is made of a horizontal flight path instead of the vertical one of Witteborn and Fairbank. One of the first drawing of the principle is reproduced in figure 1. The principle is extremely simple and comes down to measuring the ballistic trajectory of a particle and antiparticle by measuring its deflection from the horizontal at the end of a long tunnel. The measurement consists essentially out of three steps. (1) measure the "point of no gravity" at the end of the tunnel via a collimated optical beam. (2) measure the downward displacement at the end of the tunnel experienced by a collimated beam of low energy particles due to the gravitational attraction of Earth and (3) measure the displacement at the end of the tunnel experienced by a collimated beam of low energy antiparticles.

EXPERIMENT ON THE GRAVITY OF ANTIPARTICLES

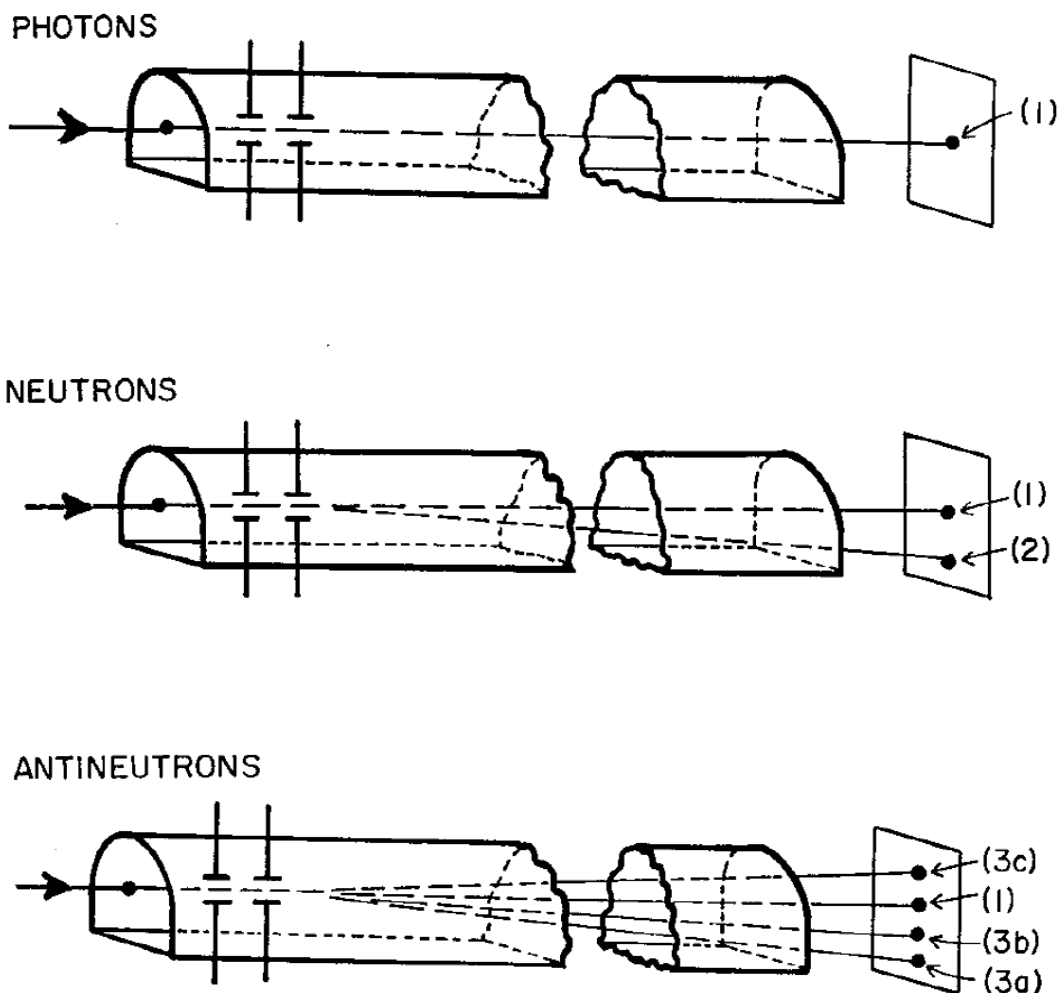


Figure 1: The experiment on the gravity on particles and antiparticles proposed by Santilli in 1994 in a long linear tunnel [20,21]. (1) measure the “point of no gravity” at the end of the tunnel via a collimated optical beam. (2) measure the downward displacement at the end of the tunnel experienced by a collimated beam of low energy particles due to the gravitational attraction of Earth and (3) measure the displacement at the end of the tunnel experienced by a collimated beam of low energy antiparticles and see whether (3a) it is the same as that of particles as generally expected or (3b) it is attractive but less than that of particles as predicted in [22] or (3c) it is a complete reversal of that of particles as predicted in [20].

Three situations can be distinguished: (3a) the measured deflection is the same as that of particles as generally expected or (3b) it is attractive but less than that of particles as predicted in [22] or (3c) it is a complete reversal of that of particles as predicted in [20]. If the deflection is measured with sufficient accuracy this experiment can decide which of the three options occurs (see also appendix D).

To prevent experimental difficulties the best way to perform this experiment is with neutral particles and antiparticles of which neutrons and antineutrons would be the best candidate.

Unfortunately, there is no proven way to slow down antineutrons. There are some ideas that slow neutrons can be transformed into slow antineutrons [23,24] but no experiment to date yielded a measurable slow antineutron flux. Second best is to use protons and antiprotons, but the efficiency of slowing down these particles and antiparticles to the ultra-low kinetic energies needed is probably the main reason why the experiments at CERN (PS200) are not continued [25,26]. The third option has no severe limitation of particle or antiparticle intensity and uses electrons and positrons. This is the option pursued here. This was the reason why Witteborn and Fairbank [18,19] used electrons and intended to use positrons in their instrument as well. Unfortunately they choose a vertical geometry for which the effect of electric field stray fields becomes much more important (as shown in appendix B).

The main cause of the failure of the Witteborn and Fairbank experiment is the smallness of the effect, similar to the force on an elementary charge due to an electric field of 6.10^{-11} V/m. This corresponds in magnitude to the repelling force between two unshielded electrons 5 m apart in vacuum. All electric fields must be eliminated or controlled within this accuracy.

Since the first attempts of Witteborn and Fairbank much effort has been invested in the study of the experimental difficulties reducing the electric field to theoretical acceptable limits. First, the focused changed from positrons to antiprotons [25,26] due to the large inertial mass difference between the elementary particles. Later, after a 1996 workshop on antimatter gravity and antihydrogen spectroscopy [27], the focused changed again to neutral antimatter. The reason for this was the problem posed by the so-called patch effects [28]. These effects were assumed to render the measurements with positrons and even with antiprotons impossible. However, Witteborn and Lockhart have always maintained that the patch effects were somehow shielded after cooling to a temperature of 4.2 K [19,29,30]. A possible shielding mechanism of the patch effect was observed by Rossi [31] and a patch effect reducing with temperature and surface treatment has been observed over a metal surface [32]. Also Dittus [33], proposing a gravity experiment in space, argues that with modern techniques the patch effect can be reduced significantly.

The above shows the need for a comparison of the gravitation on electrons and positrons and addressed why until now this has not been performed successfully. In view of the recent technological developments of surface treatment techniques and positron sources these limitations can now be overcome and the experiment by free horizontal flight in a high vacuum tube as first proposed by Santilli [20] and its principles worked out by Mills [34] can now be performed with small technological risks.

2. Principle of Santilli's proposal

2.1. Physics

The principle of Santilli's comparative test of Earth gravitation on electrons and positrons is shown in figure 1. In its principle it is a replica of the centuries-old experiments of Galilei on the motion of projectiles [35]. At one end of a well-shielded horizontal vacuum tube an electron or positron is released with a horizontal velocity, v . The particle moves through the vacuum tube until it reaches the other end at a distance L and it is detected with a position sensitive detector. During the flight the particle experiences a constant gravitational acceleration, \vec{g}_e or \vec{g}_p . The deflection at the end of the flight path is simply given by

$$\Delta y_{e,p} = g_{e,p} \frac{t^2}{2} \quad (1)$$

where t is the time the particle needs to reach the detector after it has been released at the source. This is called the time-of-flight. The deflection of the particle is proportional to the gravitational force so that measuring the deflection is sufficient to determine its sign. For neutral matter this setup can be easily realized and with some more effort the same principle has been used to detect the gravity effects on neutrons [7],[8]. The measured deflection also depends on the time-of-flight, which is simply given by L/v . Hence, the deflection is inversely proportional to the (horizontal) kinetic energy of the particle. The particle source will typically emit particles with some velocity distribution, hence the deflection is smeared out. This can be prevented by measuring the time-of-flight using a pulsed source. In that case the deflection of the particles is proportional to the square of the time-of-flight.

Another assumption in the above reasoning was that the particles are emitted horizontally. With a typical particle source this direction will have some final spread around the horizontal, which again results in smearing out of the deflection. For neutral matter this is overcome by applying a diaphragm system to direct and collimate the particle beam. As Mills [34] has shown for charged particles a diaphragm system can be replaced by a focusing system and a suitable aperture system in the middle of the flight path. This relaxes the requirements for particle source strength quite a bit as a much larger divergence can be tolerated. With the focusing lens the source is imaged on the detector reducing the smearing out of the deflection. This is schematically shown in figure 2.

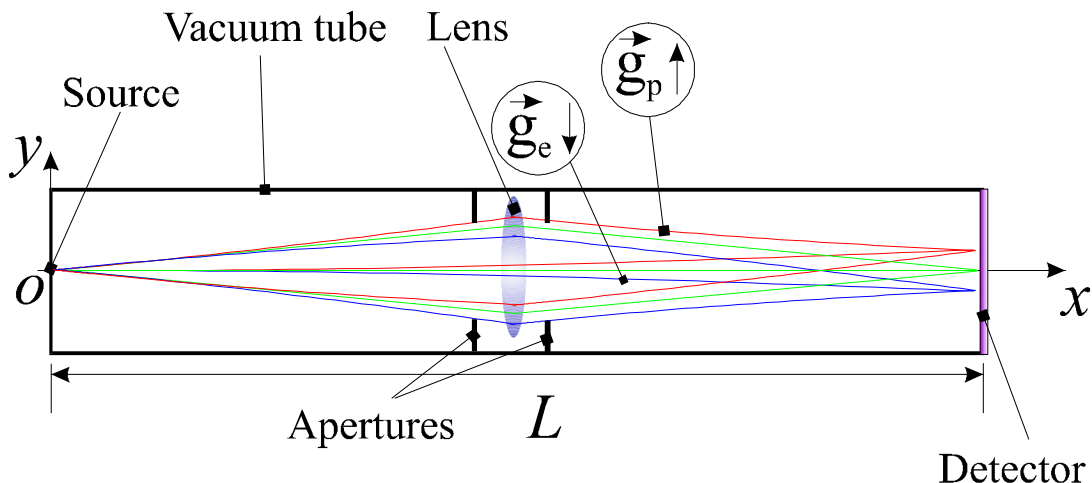


Figure 2: Principle set-up of Mills's adaptation of Santilli's comparative test of the gravity of electrons and positrons.

2.2. Measurements

The main experimental issue is how to discriminate the gravity force on electrons and positrons from forces resulting from the vertical component of the Lorentz force due to the remaining stray fields. The way this can be done is proposed by Mills [34] and shown in figure 3. The method consist of the measurement of the deflection for electrons and positrons and taking the average. The details are worked out in Appendix C. It is essential that the *effective horizontal* ($\Delta y = 0$) position at the detector is known. One should keep in mind that for an imaging system (as described in appendix A) the deflection should not be measured with respect to the *real horizontal*, but with respect to the image of the source on the image plane when gravity aberration is absent. Of coarse, if the horizontal is known together with the source positions and the imaging properties of the focusing system, this imposes no additional problem. One just takes as an effective horizontal the line through the center of the focusing system and the image.

This shows that the optical center of the imaging system must be known with the same accuracy as required for the measurement of deflection. This position can also be inferred from the parabolic behavior of the deflection (if it is assumed that all electric fields are negligible) and by rotating the complete setup around its z -axis.

If the effective horizontal is known, the average of the electron and positron deflection is independent of the static electric field and magnetic inductions as long as the gradients in these fields are small enough. Hence, the measurement procedure is as Santilli envisaged in 1994: first determine the horizontal, then the deflection of particle and antiparticle. If the remaining stray fields are too large, then take the average for comparison. The average deflection due to static field gradients depends on higher orders of the time-of-flight. This difference can be used to reduce the systematic deviations in the experiment.

The effect of the stray magnetic induction on the deflection of positrons and electrons for counter-propagating particles is precisely in opposite direction and can be cancelled if all 4 deflections are averaged. The use of multiple sources of both electrons and positrons will facilitate the control of the quality of the imaging system and will give information about the influence of any remaining stray fields.

Additional diurnal systematic effects might occur when the gravity force on electrons and positrons are opposite. A 0.24% change in deflection between noon and midnight could occur due to the different gravitation of electrons and positrons with respect to the Sun. This is worked out in appendix F.

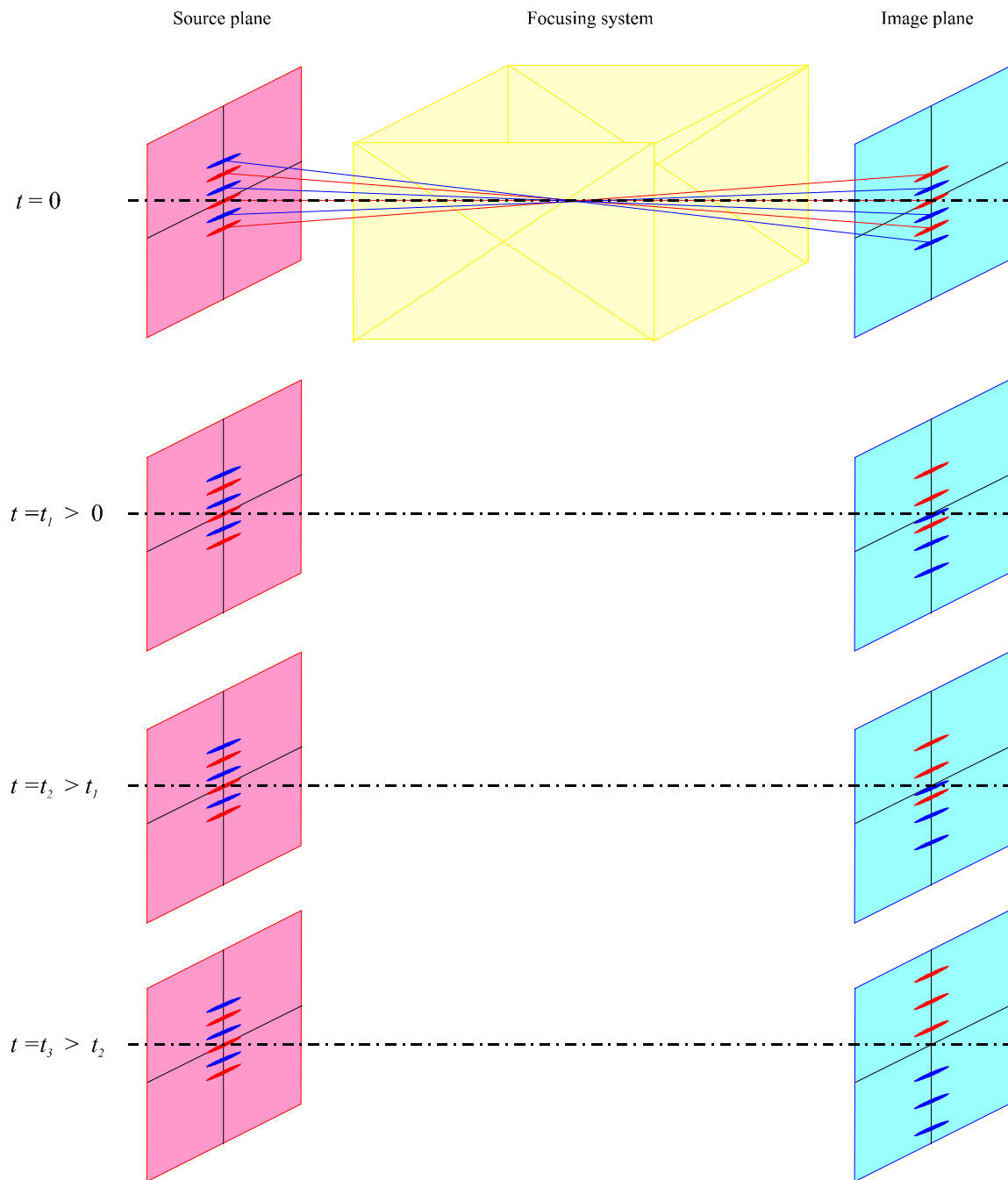


Figure 3: Example of measurement where particles fly from multiple sources (blue electron, red positron) at the source plane (left-side) via a focusing system to a position sensitive detector at the image plane for several time-of-flight moments corresponding to decreasing velocity of the particles. The lines from source plane through the optical center of the focusing system upon the image plane act as effective horizontals (see appendix C). With increasing time-of-flight the deflections are increasing with respect to the effective horizontal. In this case either upwards (red, positron) or downwards (blue, electron). The difference between deflection of electrons and positrons at a certain time-of-flight with respect to the effective horizontal only depends on the difference in gravitational attraction of the Earth and the time-of-flight.

3. Equipment

A first sketch of the instrument is shown in figure 4. The total length of the vacuum tube will be of the order of 16 m to be able to obtain a flight path of 10 m and leave some room for the installation and manipulation of sources and detectors. The sources and detectors are movable along the horizontal axis, to be able to change the focusing properties of the focusing system. The source and detector are duplicated to be able to perform measurements in both directions through the instrument. The complete setup can also be rotated around the horizontal axis. These two possibilities are used for elimination of systematic deviations. The horizontal axis is shown to stress the importance of it. The correction procedure depends critically on the known position of the horizontal (see also appendix C). The rotation of the setup around this axis enables its independent verification. Inside the vacuum tube the cooling and shielding system is incorporated to make sure that the remaining electric and magnetic stray fields are reduced to acceptable levels. The mounting of source and detector in the vacuum tube should be such that the introduction of too large electric and magnetic stray fields is prevented. The complete setup is positioned in an air conditioned room to stabilize mechanical stresses due to temperature differences.

The equipment needed can be subdivided into four categories. The first three categories are source, vacuum tube and detection. The last category entails all needed infrastructure.

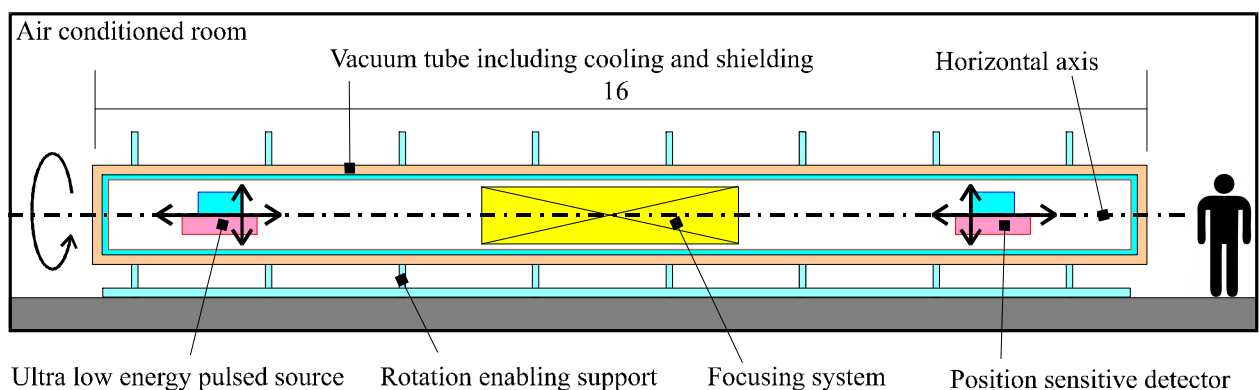


Figure 4: Sketch of proposed instrument. The sources and detectors are movable along the horizontal axis, to be able to change the focusing properties of the focusing system. The complete setup can also be rotated around the horizontal axis. These two possibilities are used for elimination of systematic deviations. The man to the right has a height of 1.8 m

3.1. Electron and positron sources

The main requirements for the electron and positron sources needed for this experiment can be inferred from figure E.2. To have a good compromise between maximal kinetic energy and minimal flight path, the available source area must have a height of some 100 μm and a width of the order of a centimeter. The width is limited by the focusing properties of the lens system. The height is limited by small kinetic energies needed. The kinetic energies needed are of the order of 1 to 100 μeV , which for electron and positron sources are ultra low energies.

That these ultra low kinetic energy electron and positron sources needed for this experiment are obtainable in sufficient quantities was shown in concept by Mills [34] (needed fast positron beam intensity of $3 \times 10^7 \text{ 1/s/cm}^2$) and by experiment as discussed by Kurz [36]. The possibilities would increase when instead of a ^{22}Na source, a reactor based positron source [37],[38] could be used where the positron yield is at least a factor of 10 larger. The need for pulses calls for an efficient use of the positrons. Hence, the best possibility is to use positron traps which can store up to 3×10^{10} positrons per cell [39] and release them in pulses. It has been shown by Weber [40] that it is possible to extract positron beams from these traps with sufficient resolution, intensity and an energy range of 200 meV with an intensity of 10^6 per pulse. If these are slowed down to the order of 100 μV , still a single pulse will contain 500 positrons.

In figure 5 a diagram of the components of the ultra-low energy pulsed positron source is sketched.

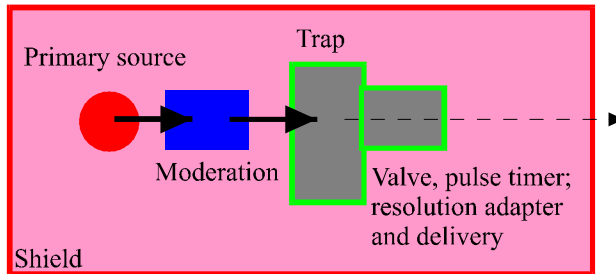


Figure 5: Diagram of the components of the ultra-low energy pulsed positron source.

3.2. Shielded vacuum tube

3.2.1. Tube length

Because of the small gravity force one could expect that the more accurate measurements are done with smaller equipment. However, just the opposite is true because of the quadratic dependence of the deflection on the length of the flight path. Because the wave character of small particles the focusing of them is imparted by Fresnel diffraction at the aperture of the lens. In appendix E it is shown that the minimal size of the aperture is fully determined by the minimal required deflection. If a deflection 'visible to the naked eye' is required (order mm) then the aperture must at least be a few centimeter and hence the flight path at least a few meter to remain in the paraxial approximation. For smaller deflections the minimal needed aperture and hence also the flight path becomes even larger to retain the focus. This seems counter intuitive as smaller deflections would mean faster particles or smaller flight path i.e. smaller flight time. However, as can be inferred from equation (E.1) a smaller flight time can only be accomplished by increasing the aperture.

A flight path as large as possible would be optimal as all other requirements relax when the flight path increases. However, the realization costs for the flight path will be roughly proportional to the square of the flight path length because, for an optimal performance, the diameter of the flight path has to be proportional to its length. If only the length will be made larger and not the diameter then the advantage of increasing the flight path is lost in the reduction of intensity. Hence, the optimal tube length depends on budget but probably will be between 10 and 100 m with a diameter of 1 to 2 m.

3.2.2. Super-cooled shielding

Probably the most crucial part of the instrument will be the shielding of residual electric fields and magnetic inductions. The most important components that need to be shielded sufficiently well are those resulting in a force in the same (or opposite) direction as gravity. An extensive review of all possible fields that need to be shielded is given by Darling [28]. His conclusion is that with the current technology it is possible to construct an adequate shielding. This has been estimated for the current case in appendix A. There it is shown that the required limits on the gradients of the electric field and magnetic induction in the gravity direction are obtainable by adequate shielding. For $L = 10$ m, $v_z = 1000$ m/s, the electric field gradient limit is $\Delta E_y / \Delta y < 2 \times 10^{-3}$ V/m² and the magnetic induction gradient limit is $\Delta B_x / \Delta y < 2 \mu\text{T}/\text{m}$. Note that these are absolute values for the gradients perpendicular to the flight path direction. The quoted limits are for gradients that are constant over the complete flight path. Local limits are much less severe, as their influence on the deflection is proportional to the square of the working distance of the gradient. Inside a multiple wall and well annealed mu-metal shield 1 meter in diameter the gradients could be as low as 1 $\mu\text{T}/\text{m}$. Today off-the-shelf superconducting shields can have a shielding factor of 10^6 at 77 K [41], which reduce Earth magnetic field (0.5 Gauss or 50 μT) to 50 pT. Specially constructed shielding as described by Mills [34] for the current case, consists of a stacked layer system of different materials cooled to a temperatures close to 4.2 K. This is shown in figure 6.

The only remaining shielding issue is the electric potential variation in the flight path of the particle due to the inner surface of the most inner layer of the flight path tube. This inner surface consists of small crystallites exhibiting a small potential variation, these constitute the so-called patch effect. This might cause a potential variation of about 1 μV on the axis of the tube. This is a reason why the inner shield must also be cooled down to liquid helium temperatures reducing the patch effects. A way of determining the influence of the patch effect is to estimate the optical phase differences due to potential variations over different paths from source to detector.

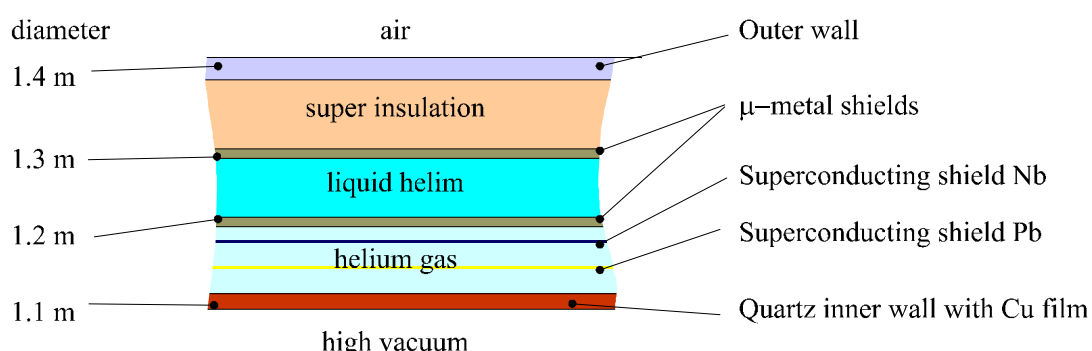


Figure 6: Principle of shielding. It consists essentially of an evacuated Helium Dewar constructed from concentric shields made of aluminum, double walls of mu-metal, double shells of superconducting Nb and Pb sheets, a quartz inner vessel and an at the inside fine-grained film of Cu.

This is described in appendix B. The conclusion is that for a horizontal flight path the patch effect is at least three orders of magnitude less important than for a vertical flight path. An additional advantage of the super-cooled conductors around the flight path is that the electric field becomes small enough so that it does not need to be compensated by additional adjustable potentials.

3.2.3. Shielding inner-surface condition

As the stray fields should be as small as possible also the remaining charged particle density must be as small as possible. As the electric field is extremely small, charged ions will slowly collect at the shields. When they make electric contact with the walls they will be neutralized. As long as they are not neutralized they will produce an disturbing electric field. When the wall is conducting, a virtual mirror charge will be induced in the wall, producing a balancing electric field. The remaining field is that of a dipole. Let us assume that a single charged ion gets stuck at a distance, ε from the surface, the remaining electric field at a distance ρ of the wall and R from the ion is given by ($\rho, R \gg \varepsilon$)

$$E = \frac{q}{4\pi\varepsilon_0 R^2} \frac{2\varepsilon}{R} \sqrt{1 + 3(\rho/R)^2}$$

which has a maximum

$$E = \frac{q}{4\pi\varepsilon_0 R^2} \frac{4\varepsilon}{R}$$

If the force on the electron of positron due to this mirror charged is to be less than the gravity force the maximum value of ε is

$$\varepsilon < \frac{4\pi\varepsilon_0 m_i g_{e,p} R^3}{q^2}$$

For $R = 0.25$ m this yields $\varepsilon < 70 \mu\text{m}$, which is easily obtainable.

Also if the walls are not conducting an image charge will build up due to the electric polarization of the wall (if the relative permittivity, ε_r , of the wall material is larger than 1). The force due to image and charge is comparable with the force of a reduced charge at the wall with reduction factor $2/(\varepsilon_r + 1)$. The gravity force corresponds in magnitude to the repelling force between two unshielded electrons 5 m apart in vacuum. Hence, for the electric field to be less than the gravity force at 0.25 m, the relative permittivity should at least be 40. Titanium dioxide has a relative permittivity of 110 and is used in white paint. It can also be sputtered in thin layers where the relative permittivity decreases a bit, but should be enough for these purposes.

3.2.4. Vacuum

The remaining gas molecules in the tube must not detrimentally disturb the flight of the electrons or positrons. If it is assumed that the mean free path for electrons and gas molecules is of the same order as the one between gas molecules

$$l = l_0 \frac{p_0}{p} \frac{T}{T_0}$$

where for Helium $l_0 = 100 \mu\text{m}$ for $T_0 = 273 \text{ K}$ and $p_0 = 100 \text{ Pa}$ and the temperature of the vacuum surroundings is liquid Helium (4.2 K) then the pressure must be maximal

$$p < \frac{l_0}{L} \frac{T}{T_0} p_0$$

where L is the length of the flight path. For $L = 10$ m this yield a maximum pressure of 1.5×10^{-8} Pa, which for cryogenic vacuum conditions is not difficult to achieve.

3.2.5. Lens system

The lens system is used to focus the source onto the imaging plane as is shown if figure 2. For a lens to work appropriate (with as small as possible aberrations) the lateral dimensions should be some two orders of magnitude smaller than the longitudinal dimensions (par-axial approximation). An additional feature of the imaging system is that the effective deflection is reduced by an amount depending on the position of the lens in the tube. This is explained in appendix A. As the focal length of a particle lens is dependent on the relative kinetic energy change of the particles, a time-of-flight dependent adaptation of the fields constituting the lens is needed. In a first approximation of the focal length, f of a magnetic lens is given by

$$\frac{1}{f} = \int \left(\frac{qB(z)}{2m_i v_z} \right)^2 dz$$

For $f = L/4 = 2.5$ m, a particle velocity of 1000 m/s and a lens region of 2.5 m, the average magnetic induction must be of the order of $\langle B \rangle = \frac{8m_i v_z}{qL} = 4.5$ nT, which is not a difficult value to obtain.

A possibility is the focusing aspects of the magnetic guide field. Another possible candidate based on electrostatic fields is an Einzel lens [42]. It has the additional advantage that a steering mechanism can be introduced. The ability to tune the lens to the right field value will determine for a large portion the minimal attainable kinetic energy or maximal attainable deflection.

3.2.6. Magnetic guide field

To keep the deflection of the electrons and positrons due to stray fields limited a static magnetic guide field must be used. The effect of the guide field is that the charged particles will spiral along the direction of the field with a spiral radius depending on the off-axis component of the particle velocity, $r = m_i v_\perp / B_z q$. At the source position the maximum off-axis component of the particle velocity is given by $v_\perp = \eta v_z / 2$, roughly determined by the aperture of the lens system. This spiral radius should be smaller than the anticipated deflection. Hence,

$$\Delta y = \frac{L^2}{v_z^2} \frac{g}{2} > \frac{\eta m_i v_z}{2qB_z} \quad \text{or} \quad B_{z,\min} = \frac{\eta m_i v_z^3}{qg L^2}$$

For $L = 10$ m, a velocity of 1000 m/s and $\eta = 0.01$ the magnetic induction of the guide field must be larger than 0.2 μ T. This can be compared to the spherical aberration due to a homogeneous magnetic field with length L where the minimal image radius to first order is given by [43]

$$r_{sf} = \left(\frac{qB_z r}{2m_i v_z} \right)^4 L$$

where r equals the distance to the optical axis. If the spherical aberration should be less than the deflection, then the maximum magnetic field is given by

$$\Delta y = \frac{L^2}{v_z^2} \frac{g}{2} > \left(\frac{qB_z \Delta y}{2m_i v_z} \right)^4 L \quad \text{or} \quad B_{z,\max} = \frac{3.36 m_i v_z^{5/2}}{q g^{3/4} L^{7/4}}$$

For $L = 10$ m and a velocity of 1000 m/s cm the magnetic induction of the guide field must be less than 2 μ T.

Hence, in the example given here, there is a possibility to apply a magnetic guide field without too much distortion of the image. The ratio between the minimum and maximum is given by

$$\frac{B_{z,\min}}{B_{z,\max}} = \frac{\eta}{2} \left(8 \frac{Lg}{v_z^2} \right)^{-\frac{1}{4}} = \eta \left(\frac{L}{\Delta y} \right)^{\frac{1}{4}}$$

and should be smaller than 1 for a suitable design, hence

$$L < \frac{\Delta y}{\eta^{\frac{1}{4}}}$$

This limits the maximum length of the flight path for a given deflection. It is also apparent that small deflections will always get blurred by a guide field, either by spherical aberration or by the spiraling path of the particles. However, as long as the above condition is satisfied the use of a magnetic guide field is possible. Here, the anticipated deflection is of the order of 1 mm and $\eta = 0.01 \dots 0.001$, hence this condition is fulfilled for $L < 10$ m.

As long as this guide field has no components in the horizontal direction perpendicular to the beam (x -direction) it does not influence the deflection in the vertical direction. The maximum value of the component in the horizontal direction can be inferred from appendix C. Equation (C.2) gives us the deflection of a constant magnetic induction over the flight path

$$\Delta y_{\max} > \frac{L^2}{v_z} \frac{q}{m_i} \frac{B_x}{2} \quad \text{or} \quad B_{x,\max} = \frac{2\Delta y_{\max}}{\frac{L^2}{v_z} \frac{q}{m_i}}$$

If the deflected beam should still hit the detector and the detector size is 10 cm, then for a flight path of 10 m and a maximum particle velocity of 1000 m/s the maximal magnetic induction in the x -direction is 10 pT. The ratio

$$\frac{B_{x,\max}}{B_{z,\min}} = \frac{g\Delta y_{\max}}{\eta v_z^2}$$

gives us a measure for the needed field homogeneity. In the example it means that the homogeneity of the guide field must be better than 50 ppm. This is rapidly relaxed for lower velocity due to the inverse-quadratic dependence. Such homogeneity is standard fabricated for NMR equipment for high fields and can be adapted for low fields also [44].

3.2.7. Magnetic field compensation

In case that not all magnetic fields are shielded, the deflection could be so large that the particles will not reach the detector. In such case the fields need to be ‘tweaked’ to reduce the deflection to acceptable values. This must be done with fields along the complete flight path as homogeneous as possible with gradients not exceeding the limits as discussed in appendix C. The magnitude and relative stability of these fields can be inferred from the previous section and should be of the order of 1 nT and 10 ppm respectively.

3.2.8. Rotation around beam axis

As the measurement procedure critically depends on the position of the effective horizontal on the detector, it is extremely important that all possible care is taken to determine its location. First off all, mechanically it can be constructed so that it is known within a few micrometer. Second, from the time dependence of the deflection the horizontal can be extrapolated. A third possibility to reduce the systematic is by rotation of the complete tube, including detector and sources around the beam axis. Any deviation in the horizontal should turn up in a different deflection result.

3.3. Detection

The preferable detector should be a linear position sensitive detector that can detect both electrons and positrons (see figure 7). The slow particles arriving at the detector should first be adapted (velocity increase) so that they can be detected by the detector, keeping the spatial information available. The spatial resolutions should be in the order of 100 μm and the time resolution of the order of 0.1 ms with an efficiency as high as possible. These are moderate requirements and can be met by for instance micro channel plates [45],[46],[47] or linear CMOS detectors [48]. One issue that must be kept in mind is that the magnetic or electric stray fields of the detector do not systematically disturb the detection position in such a way that the deflection can not be adequately detected.

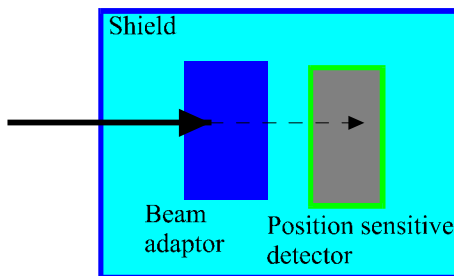


Figure 7: Diagram of the components of the position sensitive detector

3.4. Infrastructure

The infrastructure needed for the execution of the experiment is mainly the availability of liquid Nitrogen and Helium to cool the shielding. Together with this cryogenic capability a high vacuum capability is needed.

As positrons are needed it would be advantageous to work with a group where they have such capabilities or where they are allowed to handle radioactive materials, otherwise the licensing will be quite an additional expense.

An electrical and mechanical workshop would be beneficial.

The experiment would be best located in a vibration free, temperature controlled environment to limit possible drifts in equipment and to reduce mechanical and thermal stresses and gradients in the tube and shielding.

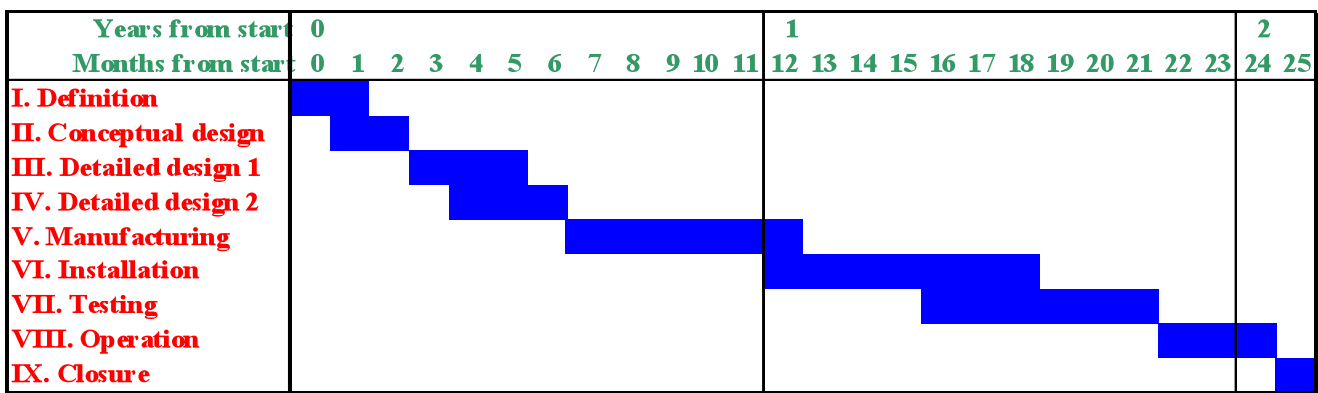


Figure 8: Initial planning of time schedule.

4. Time schedule

A rough overview of the time schedule is shown in figure 8. The schedule is divided into separate phases which all end with a go/no-go decision for the next phase. The phases entail:

Phase 1: Definition

During this phase final strategic decisions must be made concerning the capabilities of the instrument, and how to handle the issues influencing the instrumental performance. Further cooperation must be established with different suppliers for the needed infrastructure and other parts of the instrument that are not off-the-shelf apparatus, like for instance the source, focusing system and detector.

Phase 2: Conceptual design

During this phase contact will be made to potential suppliers or manufacturers of components. On the basis of the strategic decisions they are invited to make a quotation for the conceptual design of these components, including an offering for the delivery. One or more of these manufacturers will be contracted to do the conceptual design. After that a choice of manufacturer is made.

Phase 3: Detailed design 1

During this phase the chosen manufacturer(s) of the components will be notified and agree upon the first part of the detailed design. This part must generate sufficient information for starting to define the detailed requirements on infrastructure. After that, the corresponding part of the detailed design must be performed, creating the input for the optimization of these items. After that the optimization can be performed.

Phase 4: Detailed design 2

During this phase the chosen manufacturer(s) of the components will be notified and agree upon the optimization of the relevant items. Upon this agreement they can start the remaining part of the detailed design. Safety analysis and requirements must be defined and performed. The detailed design drawings and quality norms and standards for manufacturing process will be made and agreed upon.

Phase 5: Manufacturing

During this phase all parts will be manufactured, all equipment purchased and a detailed test and commissioning plan is made.

Phase 6: Installation

During this phase the installation of all systems will be performed on site. Before this can be done, first preparations must be done to make sure the site can support the instrument.

Phase 7: Testing

During this phase the testing and commissioning of the instrument will be performed. Firstly, relevant parts of the instrument will be tested separately. Secondly, complete systems will be tested. Finally, the complete assembly of systems will be tested. During commissioning operators will learn to operate the instrument.

Phase 8: Operation

During this phase the experiment will be performed, any problems that might occur are reported and if possible within budget, solved.

Phase 9: Closure

During this phase the experiment is ended and the results are handed over to the project owner. The project owner has to agree with the results of the project and decides on the closure of the project.

5. Budget

The total budget for all phases is shown in figure 9 below. Differentiation is made between design days, manufacturer days, material costs and equipment costs.

‘Design days’ is an estimate of the number of days needed for the conceptual and detailed design of the specific part. It is expressed in days to get an idea about the time span involved. At the end the design days are translated into costs by taken an average rate of 1000 euro/day.

‘Manufacturer days’ is an estimate for the number of days needed by a mechanics or electronics workshop to construct the specific part. Again it is expressed in days to get an idea about the time span involved. At the end these days are translated into costs by taken an average rate of 750 euro/day.

‘Materials’ is an estimate of the costs for the materials needed to construct the specific part. This entails the raw materials and components for producing the part.

‘Equipment’ is an estimate of the costs for equipment which can be bought from the shelve and are needed for controlling the temperature, vacuum, magnetic fields, rotation and translation axis, etc.

The cost for ‘infrastructure’ is based on an estimate for the use of the infrastructure of the hosting facility. It was estimated for a three month experiment for 5 days a week and 2000 euro costs per day. The use of the infrastructure of the facility during the installation phase was not taken into account. Also personnel costs during installation and performing of the experiment are not taken into account. For project management a total of 100 days is taken into account. The total budget is almost 2 MEuro.

	Design days	Manufact. days	Materials keuro	Equipment keuro
I. Electron and positron sources				1)
Electron primary source	1	1	10	10
Positron primary source	5	2	20	50
Adaptation primary sources	5	2	2	10
Storage	5	2	50	10
Moderation	10	10	50	50
Pulsing	5	2	10	50
Delivery	10	10	20	20
SubTotal	41	29	162	200
II. Shielded vacuum tube				
Tube length	5	20	50	150
Super-cooled shielding	10	25	70	150
Vacuum	5	5	20	50
Lens system	10	2	5	10
Magnetic guide field	5	2	10	10
Magnetic field compensation	10	10	50	50
Rotation around beam axis	5	10	100	150
SubTotal	50	74	305	570
III. Detection				
Beam adapter	5	10	5	25
Position sensitive detector	10	2	5	50
SubTotal	15	12	10	75
IV. Infrastructure				
Use of facilities				135
Project Management	100			
SubTotal	100	-	-	135
Unforeseen 10%	21	12	48	98
Total				
in days	227	127		
in keuro	227	95	525	1,078
Grand Total / keuro				1,924

1 Design day = 1000 euro

1 Manufacturing day = 750 euro

1) This depends on cooperation

2) Based on dayly costs of 2000 euro for 5 days a week for 3 months

Figure 9: Combined budget for all phases divided into needed equipment parts.

6. Existing suitable facilities

Large institutions doing fundamental research like CERN or SLAC can all provide the needed infrastructure. All well equipped universities could also support the experiment.

Groups that have experience with positron sources could be of advantage for the design of the several component:

- Positron Research group at University of California, San Diego, USA
- Positron Lab, Department of Physics and Astronomy, University of California at Riverside, 900 University Avenue, Riverside, CA 92521, USA
- Intense Positron Beam, North Carolina State University, Raleigh, NC 27695-7909, USA
- The Argonne National Laboratory Slow-Positron source (APoS), USA
- FRM II and Physics Department, Technische Universität München, Garching, Germany
- EPOS - ELBE Positron Source at Research Center Dresden / Rossendorf, Germany
- RID and FAME, Delft University of Technology, Delft, The Netherlands
- Institute of Materials Structure Science (IMSS), High Energy Accelerator Research Organization (KEK), 1-1 Oho, Tsukuba, Ibaraki 305-0801, Japan
- Atomic Physics Laboratory , RIKEN Advanced Science Institute, 2-1 Hirosawa, Wako, Saitama 351-0198 Japan
- Institute of High Energy Physics , Chinese Academy of Sciences, 19B YuquanLu, Shijingshan District, Beijing, 100049, China

References

- [1] I. Newton, *The Principia* (1687), republished in 1995 by Prometheus Books, New York
- [2] A. Einstein, *Annalen der Physik* 49 (1916) p769-822
- [3] T. J. Sumner, *Living Review Relativity* 5 (2002) 4 [Online Article]: cited on July 19, 2011, <http://www.livingreviews.org/Articles/Volume5/2002-4sumner/>
- [4] G. Bertone, D. Hooper and J. Silk, <http://arxiv.org/abs/1101.2063v1>
- [5] R. v. Eötvös, D. Pekar and E. Fekete, *Annalen der Physik* 373 (9) (1922) p11-68
- [6] P. G. Roll, R. Krotkov and R. H. Dicke, *Annals of Physics (N.Y.)* 26 (1964) p442-517
- [7] J. W. T. Dabbs, J. A. Harvey, D. Paya and H. Horstmann, *Physical Review* 139 () (1965)
- [8] L. Koester, *Physical Review D* 14 (4) (1976) p907-909
- [9] K. C. Littrell, B. E. Allman and S. A. Werner, *Physical Review A* 56 (3) (1997) p1767-1780
- [10] J.D. Barrow and R. J. Scherrer, *Physical Review D* 70 (10) (2004) 103515
- [11] M. Kowit, *International Journal of Theoretical Physics* 35 (3) (1996) p605-631
- [12] M. Doser, et al, *Journal of Physics: Conference Series* 199 (2010) p012009 (see also <http://aegis.web.cern.ch/aegis/home.html>)
- [13] A. Kellerbauer et al., *Nuclear Instruments and Methods in Physics Research B* 266 (2008) p351-356
- [14] A. D. Cronin, et al., Letter of Intent: Antimatter Gravity Experiment (AGE) at Fermilab, downloaded from <http://www.fnal.gov/directorate/programplanning/Mar2009PACPublic/AGELOIFeb2009.pdf> on Nov 29, 2010
- [15] D. M. Kaplan, New experiments with anti protons, *Nuclear Physics A* 844 (2010) p206c-215c
- [16] A. Einstein and N. Rosen, *Physical Review* 48 (1935) p73-77
- [17] R. M. Santilli, Isodual Theory of Antimatter, in: *Fundamental Theories of Physics* 151, editor A. van der Merwe, Springer, Dordrecht, The Netherlands (2006) ISBN-101-4020-4517-4
- [18] F. C. Witteborn and W. M. Fairbank, *Physical Review Letters* 19 (18) (1967) p1049-1052
- [19] F. C. Witteborn and W. M. Fairbank, *Review of Scientific Instruments* 48 (1) (1977) p1-11
- [20] R. M. Santilli, Antigravity, *Hadronic Journal* 17 (1994) p257
- [21] R. M. Santilli, Elements of Hadronic Mechanics, Vol.II, Theoretical Foundations, Academy of Sciences of the Ukraine, Kiev, 1994
- [22] M. M. Nieto and T. Goldman, *Physics Reports* 205 (1991) p221 and 216 (1991) p345 (1992)
- [23] H. Yoshiki and R. Golub, Ultra-Cold Anti-Neutrons (II) Production probability under magnetic and gravitational fields, *Nuclear Physics A* 536 (1992) p648-668
- [24] T. Bressani and A. Filippi, Antineutron physics, *Physics Reports* 383 (2003) p213-297
- [25] T. Goldman and M. M. Nieto, Experiments to measure the gravitational acceleration of antimatter, *Physics Letters* 112B (6) (1982) p437-440
- [26] T. Goldman et al., Beyond metric gravity: Progress on PS-200 Hyperfine Interactions 81 (1993) p87-96
- [27] M. H. Holzscheiter, Workshop summary, International workshop on antimatter gravity and anti hydrogen spectroscopy, Sepino Molise, Italy, 19-25 May 1996, *Hyperfine Interactions* 109 (1997)
- [28] T. W. Darling, F. Rossi, G. I. Opat and G. F. Moorhead, The fall of charged particles under gravity: A study of experimental problems, *Review of Modern Physics* 64 (1) (1992) p237-257
- [29] J. M. Lockhart, F. C. Witteborn and W. M. Fairbank, Evidence for a Temperature-Dependent Surface Shielding Effect in Cu, *Physical Review Letters* 38 (21) (1977) p1220-1223
- [30] J. M. Lockhart, F. C. Witteborn and W. M. Fairbank, Errata, Evidence for a Temperature-Dependent Surface Shielding Effect in Cu, *Physical Review Letters* 67 (2) (1991) p283
- [31] F. Rossi and G. I. Opat, Observations of the effects of adsorbates on patch potentials, *Journal of Physics D: Applied Physics* 25 (1992) p1349-1353

- [32] J. Labaziewicz, Y. Ge, D. R. Leibrandt, S. X. Wang, R. Shewmon and I. L. Chuang, Temperature Dependence of Electric Field Noise above Gold Surfaces, *Physical Review Letters* 101 (2008) p180602-1-4
- [33] H. Dittus, C. Lämmerzahl and H. Selig, Testing the Universality of Free Fall for Charged Particles in Space, *General Relativity and Gravitation* 36 (3) (2004) p571-591
- [34] A. P. Mill Jr., Possibilities for measuring the passive gravitational mass of electrons and positrons in free horizontal flight, *Hadronic Journal* 19 (1996) p77-86
- [35] G. Galilei, *Dialogues Concerning Two New Sciences* (1638), republished by Great Minds Series, Translated by H. Crew and A. de Salvio, Prometheus Books, New-York, 1998
- [36] C. Kurz, S. J. Gilbert, R. G. Greaves and C. M. Surko, New source of ultra-cold positron and electron beams, *Nuclear Instruments and Methods in Physics Research B* 143 (1998) p188-194
- [37] A. van Veen, H. Schut, J. de Roode, F. Labohm, C. V. Falub, S. W. H. Eijt and P. E. Mijnarends, Intense positron sources and their applications, *Materials Science Forum* 363-3 (2001) p415-419
- [38] C. Hugenschmidt, G. Kögel, R. Repper, K. Schreckenbach, P. Sperr, B. Strasser and W. Triftshäuser, NEPOMUC. The new positron beam facility at FRM II, *Materials Science Forum* 445-446 (2004) p480-482
- [39] J. R. Danielson, T. R. Weber and C. M. Surko, Next Generation Trap for Positron Storage, *Non-Neutral Plasma Physics VII*, 9th International Workshop on Non- Neutral Plasmas, edited by J. R. Danielson and T. S. Pedersen, (2009) p199-206
- [40] T.R. Weber, Tailored Charged Particle Beams from Single-Component Plasmas, PhD Thesis, University of California, San Diego (2010).
- [41] See for instance <http://www.can-superconductors.com/products/magnetic-shields/>
- [42] P. Mandala, G. Siklerb and M. Mukherjeea, Simulation study and analysis of a compact Einzel lens-deflector for low energy ion beam, *Journal of Instrumentation* 6 (2011) p02004
- [43] K.D. van der Mast and W.Chr. Heerens, *Inleiding deeltjes optica*, 3e volledig herziene druk Delft University of Technology section Deeltjesoptica (1997)
- [44] See for instance <http://www.cryomagnetics.com/>
- [45] J. L. Wiza, Microchannel plate detectors, *Nuclear Instruments and Methods* 162 (1979) p587-601
- [46] P.Y. Schmidt et al., An efficient position sensitive detector for 3-30 keV positrons and electrons, *Nuclear Instruments and Methods in Physics Research A* 376 (1996) p139-145
- [47] ALPHA Collaboration, G. B. Andresen et al., Antiproton, positron, and electron imaging with a microchannel plate/phosphor detector, *Review of Scientific Instruments* 80 (2009) p123701-1-5
- [48] See for instance <http://www.scmos.com/>

Summary

It is astonishing that even after more than three centuries after the grounding experiments of Galilei [35] and the scientific synthesis of Newton [1] the influence of Earth gravitation on elementary charged particles and antiparticles is still unknown. This proposal shows that it is now possible for reasonable costs and effort to fill this gap in human knowledge.

After an historic introduction and the reason for the necessity of the proposed experiment, a scientific description of Santilli's comparative test of the gravity of electrons and positrons in a horizontal super-cooled vacuum tube is given. The test is a decisive experiment about the difference between the gravity force on electrons and positrons due the gravitation of Earth.

The main issues that make the experiment difficult are the needed ultra low energy electrons and positrons and the shielding of stray electric and magnetic fields. Its is shown that with current technology these issues can be overcome in two years time with an investment of 2 MEuro.

Appendix A: Gravity aberration of a perfect particle lens

Gravity curves the path of particles through a perfect lens. Due to this curvature the image through a perfect lens changes so that an aberration effect is introduced.

Curved trajectory of particle

The classical path of a particle due to a gravity force $mg_{e,p}\vec{e}_y$ can be described by

$$y_{\max} - y = \frac{(x - x_{\max})^2}{4H}$$

where (x_{\max}, y_{\max}) are the coordinates of the maximum of the trajectory and

$$H = \frac{v_x^2}{2g} = \frac{h^2}{2gm^2\lambda^2}$$

where v_x equals the horizontal velocity, λ the wavelength of the particle at this maximum, g the acceleration due to gravity, m the inertial mass of the particle and h is Plank's constant. The slope of the trajectory is given by

$$\frac{dy}{dx} = \frac{k_y}{k_x} = \frac{x_{\max} - x}{2H}$$

where k_x, k_y are the horizontal and vertical components of the wave vector. Hence, the magnitude of the wave vector is given by

$$k^2 = k_x^2 + k_y^2 = k_x^2 \left(1 + \left(\frac{x_{\max} - x}{2H} \right)^2 \right) = k_x^2 \left(1 + \frac{y_{\max} - y}{H} \right)$$

equal to the wave vector derived from the Schrödinger equation. x_{\max} and y_{\max} can be expressed in the slope $\tan \xi_1$ at some coordinates (x_1, y_1) of the path, yielding

$$x_{\max} = x_1 + 2H \tan \xi_1$$

and

$$y_{\max} = y_1 + H \tan^2 \xi_1$$

so that

$$y = y_1 + (x - x_1) \left(\tan \xi_1 - \frac{x - x_1}{4H} \right)$$

and

$$\frac{dy}{dx} = \tan \xi_1 - \frac{x - x_1}{2H}$$

Refraction at a perfect thin lens

A perfect thin lens refracts the incident beam by an angle θ towards the beam axis at the location of the lens. The incident beam has an angle α with the optical axis. Then, the angle of the refracted beam with the optical axis β is given by

$$\beta = \alpha - \theta = \alpha - \frac{h}{f}$$

where h equals the distance between the optical center of the lens (focal length f) and the intersection of the incident beam with the lens (see figure A1). In case of straight trajectories of the particles before and after the lens, this can be derived from the lens formula (paraxial approximation).

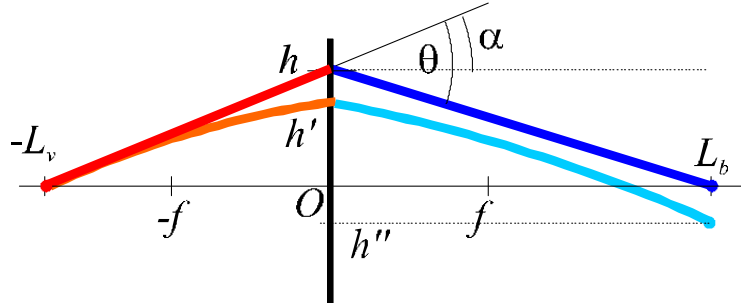


Figure A1: Refraction of particle at thin lens.

Now, assume that at the object point at a distance L_v before the lens, a particle is emitted with an angle $\alpha = h/L_v$. Due to gravity the trajectory becomes curved and the direction of the particle at the intersection with the lens has changed to

$$\alpha' = \alpha - \frac{L_v}{2H}$$

Notice that $\tan \alpha'$ is approximated by α' , which is allowed because of the paraxial approximation. The distance to the optical axis has become

$$h' = L_v \left(\alpha - \frac{L_v}{4H} \right)$$

Hence, after refraction the angle of the trajectory is changed to

$$\beta' = \alpha' - \frac{h'}{f} = \left(1 - \frac{L_v}{f} \right) \alpha + \frac{L_v}{2H} \left(\frac{L_v}{2f} - 1 \right)$$

Again, due to gravity the trajectory of the refracted particle becomes curved and the direction of the particle at the image position has changed to

$$\beta'' = \beta' - \frac{L_b}{2H}$$

where L_b equals the image distance. The distance to the optical axis has become

$$h'' = h' + L_b \left(\beta' - \frac{L_b}{4H} \right)$$

If it is assumed that $L_b = f L_v / (L_v - f)$, then

$$\beta'' = \left(1 - \frac{L_v}{f} \right) \alpha + \frac{L_v}{2H} \left(\frac{L_v}{2f} - 1 - \frac{f}{L_v - f} \right)$$

and

$$h'' = -\frac{L_v^2}{4H} \frac{f L_v}{(L_v - f)^2}$$

The drop of a particle emitted in the horizontal direction at $x = -L_v$ when it reaches the image position without a lens is

$$\Delta y = -\frac{L_v^2}{4H} \frac{L_v^2}{(L_v - f)^2}$$

so that

$$\frac{h''}{\Delta y} = \frac{f}{L_v}$$

Hence, the expected deviation due to gravity is reduced by the imaging of the thin lens, by a factor determined by the ratio between the focal distance of the lens and the object distance. If it is assumed that $L_b = L_v = 2f$, then the deviation is halved.

Gravity distorted image by a perfect thin lens

The above derivation can be generalized to an image of an object at some distance above the optical axis (see figure A2).

It can be shown that the image distance L_b is not changed by gravity, but the distance to the optical axis of the image is changed to

$$H_c = H_b - h'' = H_b - \Delta y \frac{f}{L_v}$$

where

$$\frac{H_b}{H_v} = \frac{f}{L_v - f}$$

is the image magnification factor.

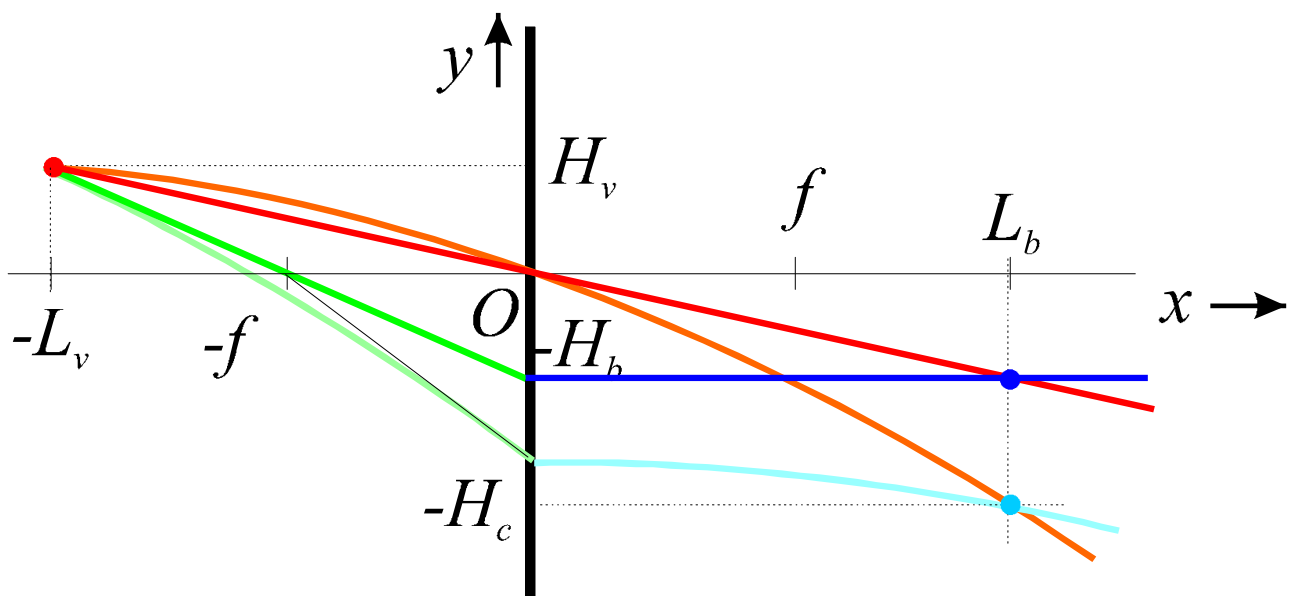


Figure A2: Image distortion due to gravity of an object at some distance above the optical axis.

Appendix B: Surface patch potential effect

The most important shielding issue is the electric potential variation in the flight path of the particle due to the inner surface of the most inner layer of the flight path tube [28]. This inner surface consists of small crystallites exhibiting a small potential variation, these constitute the so-called patch-effect. This might cause a potential variation of about 1 μ V on the axis of the tube.

Optical phase

A way of determining the influence of the patch effect is to estimate the optical phase differences due to potential variations over different paths from source to detector. The optical phase along a particle trajectory is given by

$$\psi = \frac{2\pi}{\lambda} \oint n(\vec{s}) d\vec{s}$$

where $n(\vec{s})$ equals the refractive index along the trajectory defined by \vec{s} and λ the wavelength of the particle. This refractive index is coupled to the potential by

$$n(\vec{s})^2 = 1 \pm \frac{2em\lambda^2}{h^2} V(\vec{s})$$

where $e = 1.602 \times 10^{-19}$ C is the elementary charge, m the inertial mass of the particle. h is Plank's constant and $V(\vec{s})$ is the potential along the trajectory. The plus holds for electrons, the min for positrons. Variations in the potential due to the patch effect are very small, hence the variations in the refractive index can be approximated by

$$\Delta n(\vec{s}) = \pm \frac{em\lambda^2}{h^2} \Delta V(\vec{s})$$

and variations in the optical phase are directly related to variations in the potential according to

$$\Delta\psi = \pm 2\pi \frac{em\lambda}{h^2} \oint \Delta V(\vec{s}) d\vec{s}$$

Magnitude

According to Darling [28] a Gaussian distributed patch effect (with root-mean-square patch potential, φ_p and average crystallite size ξ on the inner surface of a long cylinder $L \gg D$) results in potential variations of $2\varphi_p\xi/D$ on the axis. The line integral over these variations can be estimated by transforming the integral over a sum of L/ξ patches of length ξ . The sum can be regarded as a random walk, so that the final spread in ψ becomes

$$\frac{\sigma_\psi}{2\pi} = \frac{\lambda}{\lambda_0} \frac{\varphi_p \xi \sqrt{L\xi}}{P_0 D} < 1 \quad (\text{B.1})$$

where $\lambda_0 = 100$ nm and

$$P_0 = \frac{h^2}{2em\lambda_0} = 1.5 \times 10^{-11} \text{ Vm}$$

To be able to get a good focus this variation in optical phase should be much smaller than 2π . Note that the variation is proportional to the wavelength, which clearly favors faster particles. For a shielding with a diameter of 1 m and a length of 10 m, for electrons of 1 μ m and a patch length of 1 μ m the patch potential has to be less than 500 μ V, which is perfectly feasible [32].

Witteborn and Fairbank experiment

According to equation (B.1) the spread in optical phases close to the cylinder axis is proportional to the wavelength. This explains why the vertical flight path as used by Witteborn [18,19] is much more sensitive to the patch effect than the horizontal flight path considered here. Take

$\lambda = \lambda_0 v_0 / \sqrt{gL}$ where $v_0 = 7.27$ km/s is the velocity of an electron with wavelength λ_0 . Thus λ is the average wavelength for a particle just reaching the top of the flight path. Then for $L = 1$ m, $D = 4$ cm and $\xi = 1$ μm , φ_p has to be less than 250 nV at least a factor of 2000 smaller.

Darling [26] takes $\xi \ll 1$ nm and $\varphi_p = 0.01$ V, as limit which corresponds to a variation of the optical path phase of $\sigma_\psi \ll 2.4\pi$. Hence, both approaches give similar results.

Magnitude for constant deflection

Equation (B.1) can be rewritten as function of the total deflection of the particle beam

$$\frac{\sigma_\psi}{2\pi} = \frac{2e}{h} \sqrt{\frac{2\Delta y}{g}} \frac{\varphi_p \xi \sqrt{\xi}}{D\sqrt{L}} \quad (\text{B.2})$$

This is independent of the particle properties. Hence, *for a required given deflection in the proposed experiment, the influence of the patch potential effects does not depend on the type of particle used.*

In view of the relatively large kinetic energies involved in this horizontal flight path experiment with regard to the Witteborn and Fairbank experiment [18] and the implicit determination of the average kinetic energy by means of the time-of-flight method, the influence of the patch-effects will be much reduced.

This also relaxes the requirements on the vacuum pressure quality to about 10^{-8} Pa as the time-of-flight is at least a factor of 100 shorter and the main effect it has on the results is a reduced intensity at the detector.

Appendix C: Gravity deflection measurement procedure

Mills' gravity deflection measurement [34] consist of the measurement of the deflection for 4 different situations and taking the average. If the horizontal is known, the average is independent of the average electric field and magnetic induction. The average deflection due to gravity has a parabolic dependence on the time-of-flight. The average deflection due to constant field gradients depend on higher even orders of the time-of-flight. This difference can be used to reduce the systematic deviation in the experiment. The required limits on the gradients of the electric field and magnetic induction in the gravity direction are obtainable by adequate shielding.

Vertical force on charged particle

The vertical force on a charged particle (charge q , inertial mass m , gravitational acceleration g) traveling in the horizontal (z) direction and subject to a vertical electric field E_y and a horizontal magnetic induction B_x perpendicular to the beam is given by

$$F_y = -mg + qE_y + qv_z B_x = m \frac{d^2 y}{dt^2} \quad (\text{C.1})$$

where E_y and B_x depend on x, y, z . This force accelerates the particle in the direction of F_y , hence the deflection after a time t is given by

$$\Delta y = \frac{1}{m} \int_0^t \int_0^t F_y dt'' dt'$$

which can be rewritten as

$$\Delta y = \frac{L^2}{v_z^2} \left\{ -\frac{g}{2} + \frac{q}{m} \varepsilon + \frac{qv_z}{m} \beta \right\} \quad (\text{C.2})$$

where

$$\varepsilon = \frac{1}{L^2} \int_0^L \int_0^z E_y(x', y', z') dz' dz$$

and

$$\beta = \frac{1}{L^2} \int_0^L \int_0^z B_x(x', y', z') dz' dz$$

are the field averages over the trajectories followed by the particles.

Constant fields

In lowest order, if variations in E_y and B_x are neglected, these are just constants. Now if the sum is taken of the positron deflection (charge $+e$, gravitational acceleration g_p) and electron deflection (charge $-e$, gravitational acceleration g_e) the result is

$$\Delta y_p + \Delta y_e = -\frac{L^2}{v_z^2} \frac{g_p + g_e}{2}$$

independent of the constant value of E_y and B_x . Note that this deflection is parabolic in the time-of-flight which gives a possibility to check the systematic deviations of the experiment. Further, as anticipated by Santilli in 1994 [20,21] it is essential that the horizontal ($\Delta y = 0$) position at the detector is known. This position can be inferred from the parabolic behavior of the deflection and by rotating the complete setup around its z -axis. A further check on systematic deviations is to reverse the flight direction, keeping all other conditions the same, so that v_z is replaced by $-v_z$ in

the above equation and the effect of the magnetic induction is canceled when the average of the deflections is taken. One should keep in mind that for an imaging system (as described in appendix A) the deflection should not be measured with respect to the horizontal, but with respect to the image of the source on the image plane when gravity aberration is absent. Of course if the horizontal is known together with the source positions and the imaging properties of the focusing system this imposes no additional problem. One just takes as an *effective horizontal* the line through the center of the focusing system and the image. This shows that the optical center of the imaging system must be known with the same accuracy as required for the deflection.

Horizontal gradient in fields

To first order, horizontal variations in E_y and B_x (as function of z) can be incorporated, while variation in the y -direction is neglected. Then

$$E_y(z) = E_y(0) + \frac{z}{L} (E_y(L) - E_y(0))$$

and

$$B_x(z) = B_x(0) + \frac{z}{L} (B_x(L) - B_x(0))$$

so that

$$\varepsilon = \frac{2E_y(0) + E_y(L)}{6}$$

and

$$\beta = \frac{2B_x(0) + B_x(L)}{6}$$

again constants. This holds for all variations as function of z . Hence, the same averaging procedure gives the same result.

Vertical gradient in fields

To first order, vertical variations in E_y and B_x (as function of y) can be incorporated. Then

$$E_y(y) = E_y(0) + \frac{y}{y_m} (E_y(y_m) - E_y(0))$$

and

$$B_x(y) = B_x(0) + \frac{y}{y_m} (B_x(y_m) - B_x(0))$$

so that

$$\varepsilon = \frac{2E_y(0) + E_y(L)}{6}$$

and

$$\beta = \frac{2B_x(0) + B_x(L)}{6}$$

Then, from equation (C.1)

$$\frac{d^2y}{dt^2} = -g + a - by$$

where

$$a = \frac{q}{m} (E_y(0) + v_z B_x(0))$$

and

$$b = -\frac{q}{m} \frac{E_y(y_m) - E_y(0) + v_z(B_x(y_m) - B_x(0))}{y_m}$$

Note that both a and b change sign if the charge of the particle is reversed. When using the correct initial conditions ($y(0)=0$ and $v_y(0)=0$) then if $b \geq 0$

$$y(t) = (a-g) \frac{t^2}{2} \left(\frac{\sin \frac{t\sqrt{b}}{2}}{\frac{t\sqrt{b}}{2}} \right)^2 = (a-g) \frac{t^2}{2} \left(1 + \frac{bt^2}{12} + O^2\left(\frac{bt^2}{12}\right) \right)$$

and if $b < 0$

$$y(t) = (a-g) \frac{t^2}{2} \left(\frac{\sinh \frac{t\sqrt{-b}}{2}}{\frac{t\sqrt{-b}}{2}} \right)^2 = (a-g) \frac{t^2}{2} \left(1 + \frac{bt^2}{12} + O^2\left(\frac{bt^2}{12}\right) \right)$$

Now if the sum is taken of the positron and electron deflection the result is

$$\Delta y_p + \Delta y_e = -\frac{t^2}{2} \left[g_p + g_e + (g_p + g_e - 2a) \frac{bt^2}{12} - (g_p + g_e) O^2\left(\frac{bt^2}{12}\right) \right]$$

Except for a parabolic dependence on the time-of-flight, also higher orders of the time of flight can be distinguished. If the correction term needs to be small then $|bt^2| < 1$, which gives a criterion for the maximum gradient in either electric field or magnetic induction. For $L = 10$ m, $v_z = 1000$ m/s, $b < 10^4$ 1/s, hence $\Delta E_y / \Delta y < 2 \times 10^{-3}$ V/m² and $\Delta B_x / \Delta y < 2 \mu\text{T}/\text{m}$.

Note that these are absolute values for the gradients perpendicular to the flight path direction. The quoted limits are for gradients that are constant over the complete flight path. Local limits are much less severe, as their influence on the deflection is proportional to the square of the working distance of the gradient.

Inside a multiple wall and well annealed mu-metal shield 1 meter in diameter the gradients could be as low as 1 $\mu\text{T}/\text{m}$. Electric field gradients are more difficult because changes of work function are typically 0.1 V from patch to patch and can vary over large regions because of strain or surface composition. This is discussed in Appendix B.

Appendix D: Decisive outcome

It must be emphasized that only the difference between the gravity force on electrons and positrons can be detected, because of uncertainties in the value of the electric fields and magnetic inductions that remain after shielding. The experiment will result in an average deflection which will be proportional to the sum of gravitational acceleration of positrons and electrons: i.e. it will measure

$$\frac{g_p + g_e}{2}$$

where g_e is the electron gravitational acceleration and g_p is the positron gravitational acceleration. The experiment will give a definite answer to the three options as put forward by Santilli [20,21], for instance in the figure caption of figure 1 describing his proposal. These three options are:

- a) whether the Earth gravity force on electrons and positrons is the same as generally expected (i.e. $g_p = g_e$)
- b) whether the Earth gravity force on positrons is less than that on electrons as predicted by Nieto and Goldman [22] (i.e. $g_p < g_e$)
- c) whether the Earth gravity force on positrons is in the opposite direction and of equal magnitude than that on electrons as predicted by Santilli [20] (i.e. $g_p = -g_e$)

As the experiment yields: $\frac{g_p + g_e}{2}$, in the three cases we will measure:

- a) g_e
- b) $< g_e$
- c) 0

To discriminate between result a) and c) a confidence level of 99 % is needed, hence an interval of 3 standard deviations. This means that a measurement accuracy (i.e. standard deviation in the results) better than 33 % is needed. If such an accuracy is obtained then either option a) or c) is ruled out. Option b) is not a quantitative prediction and hence can not be ruled out by any experiment. It can only be confirmed and therefore it depends on the outcome. Option c) entails also option b). Option b) is not considered further.

Hence, to be 'resolutionary' between option a) and c), a measurement accuracy of at least 33% is needed. There is one experiment in literature that is somewhat comparable to the one proposed here and that is the Witteborn and Fairbank experiment. They claim to have acquired an accuracy of 10%, but they only did the experiment for electrons.

There is no principle reasons why this required accuracy could not be obtained, but at this stage it is extremely hard to predict the measurement accuracy that will be obtained.

Of coarse the aim is to make it good enough and the components of the system must be designed to obtain this accuracy. But it is not a-priori certain that this limit is reached in view of the inexperience with the complex interactions between the several elements of the experiment (for instance the electron and positron source, time-of-flight technique and flight path, electromagnetic lens, detector) and the limited resources.

However, the measurement accuracy can be determined from the experiment itself and hence the possible outcome of the experiment within a limited budget is:

either an experimental exclusion of option a) or c) , if it the accuracy is better than 33% or the accuracy is worse than 33%. In this case neither option can be excluded for 99% , but it will be clear how to increase the accuracy to obtain the 33%.

Although the first option is the targeted one, it is possible that only the second option is obtained. In that case the experiment needs additional resources and should be extended to become decisive.

Appendix E: Optimal size

An important design criterion is the wavelike structure that electrons and positrons exhibit. The De Broglie wavelength is inversely proportional to the velocity given by

$$\lambda = \frac{h}{m_i v} = \frac{\lambda_0 v_0}{v}$$

where $h = 6.626 \times 10^{-34}$ Js, $m_i = 9.109 \times 10^{-31}$ kg is the electron (or positron) inertial mass, $\lambda_0 = 100$ nm for $v_0 = 7.27$ km/s. Due to this wavelike structure of the particles, the circular apertures in the middle of the setup result in a Fraunhofer diffraction pattern at the detector plane.

The most simple diffraction pattern from a circular aperture with diameter D is the Airy pattern where the inner most intense fringe is called the Airy disk. This Airy disk has a diameter of

$$d = 1.22\lambda \frac{L}{D} = 1.22 \frac{\lambda_0 v_0}{v} \frac{L}{D}$$

as long as $D \gg \lambda$. Note that the Airy disk size is inversely proportional to the velocity of the particles, while the deflection is inversely proportional to the square of the velocity. The diameter of the Airy disk should be less than the anticipated deflection (Rayleigh's criterion), hence

$$t = \frac{L}{v} > 2.44 \frac{\lambda_0 v_0}{D |g_{e,p}|} \approx \frac{D_0 t_0}{D} \quad (\text{E.1})$$

where $D_0 = 10$ cm and $t_0 = 1.81$ ms. Hence, due to the wavelike nature of the particles, the minimal time-of-flight needed to obtain a sufficient resolution is inversely proportional to the diameter of the aperture. Note that for $L = 13$ m and $D = 10$ cm, the velocity of the particle should be maximal 7.3 km/s, hence its wavelength at least 100 nm and its corresponding kinetic energy maximal 150 μ eV. In such a case the deflection would be minimal 16 μ m. The deflection increases to 0.1 mm for particles with a kinetic energy of 25 μ eV. If one would take the values used by Mills [25] $L = 100$ m and $D = 10$ cm, then the velocity of the particle should be maximal 55.2 km/s, hence its wavelength at least 13 nm and its corresponding kinetic energy maximal 8.7 meV. In such a case the minimal deflection would still be only 16 μ m. The deflection would however increase to 5.6 mm for particles with a kinetic energy of 25 μ eV.

In reality the source will have a finite dimension, increasing the above mentioned spot diameter. For an ideal instrument the image of the source on the detector plane and the Airy disk should have approximately the same size and be comparable to the detector resolution. In such a case the minimal needed aperture is completely determined by the needed resolution or minimal deflection, Δy_{\min}

$$D_{\min} = 1.73 \frac{\lambda_0 v_0}{\sqrt{\Delta y_{\min} |g_{e,p}|}}$$

For a required minimal deflection, this minimum is completely determined. This is shown in figure E.1. This also fixes the minimal needed length of the instrument as $\eta = D/L$ is between 0.1 and 0.001. The upper bound is due to limitation of the particle-optics components (par-axial approximation) and the lower bound due to intensity limitation as the particle intensity on the detector is given by all the particles that are passed through the aperture and is proportional to η^2 , hence η cannot be made too small.

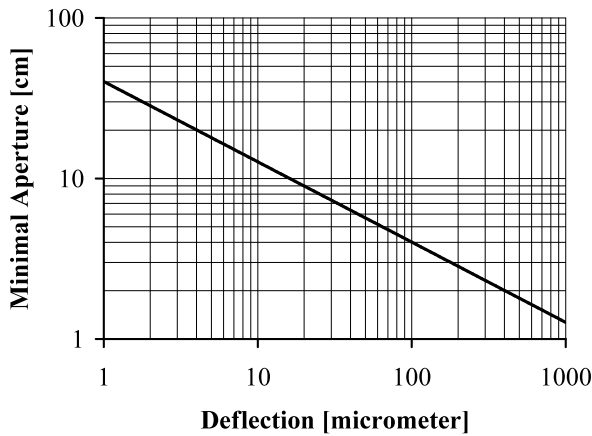


Figure E.1. Graph of the minimal aperture as function of minimal deflection in a gravity experiment to assure sufficient spatial resolution.

The maximum velocity to obtain a sufficient resolution is given by

$$v_{\max} = \frac{1.22}{\eta} \frac{\lambda_0 v_0}{\Delta y_{\min}}$$

and the corresponding maximal kinetic energy

$$E_{\max} = 0.74 m_i \left(\frac{1}{\eta} \frac{\lambda_0 v_0}{\Delta y_{\min}} \right)^2$$

The maximal kinetic energy of the particle as function of the minimal deflection is shown in the left graph of figure E.2 for different values of η . The corresponding minimal length of the flight path is shown in the right graph. From these graphs one can see that the choices made by Santilli and Mills to use a flight path between 10 and 100 m is a good compromise between the needed flight path (as small as possible) and the needed minimal kinetic energy (as large as possible).

A flight path as large as possible would be optimal as all other requirements relax when the flight path increases. However, the realization costs for the flight path will be roughly proportional to the square of the flight path length because for an optimal performance the diameter of the flight path has to be proportional to its length. If only the length will be made larger and not the diameter then the advantage of increasing the flight path is lost in the reduction of intensity. Hence, the optimal flight path depends on budget but probably will be between 10 and 100 m.

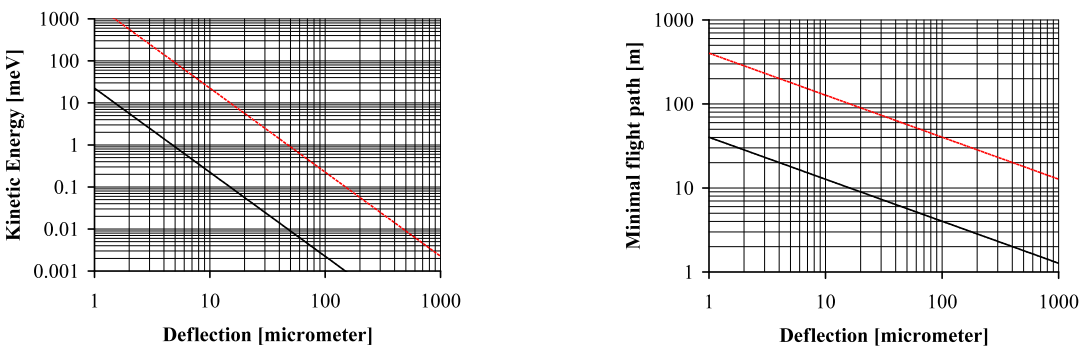


Figure E.2. Left: Graph of the maximal kinetic energy of the particles as function of minimal deflection in a gravity experiment to assure sufficient spatial resolution. Right: Graph of the minimal needed flight path as function of the same. Solid black line for $\eta = 0.01$; dashed red line for $\eta = 0.001$ (see text).

Appendix F: Influence of Sun and Moon

In case the gravity force of matter and antimatter has the same magnitude but different sign as predicted by Santilli [20], Earth, Moon and Sun will repulse the positrons. In that case an additional deflection occurs in the trajectory of the positrons with respect to the electrons. The forces on Earth bound electrons and positrons are shown in figure F.1.

The sum of the gravity force from the Sun and the centripetal force keeping the electron in its orbit around the Sun is exactly zero. Hence, the effective gravity force on the electron is just due to Earth gravitation. The positron however is not in orbit around the Sun as it is repelled. Hence, the effective gravity force on the positron is the sum of the gravity forces of the Sun and Earth and the centripetal force keeping the Earth in its orbit. Hence,

$$F_{\text{positron}} = \left| \vec{F}_{g,\text{Earth}} + \vec{F}_{cp,\text{positron}} + \vec{F}_{g,\text{Sun}} \right| = \left| \vec{F}_{g,\text{Earth}} + 2\vec{F}_{g,\text{Sun}} \right| = -m_p g \left\{ 1 + \frac{2G}{g} \frac{M_{\text{Sun}}}{R_{\text{orbit}}^2} \cos\left(2\pi \frac{t}{T}\right) \right\}$$

where $G = 6.673 \times 10^{-11} \text{ m}^3/\text{kg s}^2$ is Newtonian constant of gravitation, $M_{\text{Sun}} = 1.9891 \times 10^{30} \text{ kg}$ equals the mass of the Sun, $R_{\text{orbit}} = 1.496 \times 10^{11} \text{ m}$ equals the radius of Earth's orbit around the Sun and $T = 24.00$ hours and t is the local time of day. The second term varies with the local time of day and has an amplitude of 0.12 % and the difference between day and night is 0.24 %.

A similar calculation can be done for the Moon, which yields an amplitude of only 7 ppm.

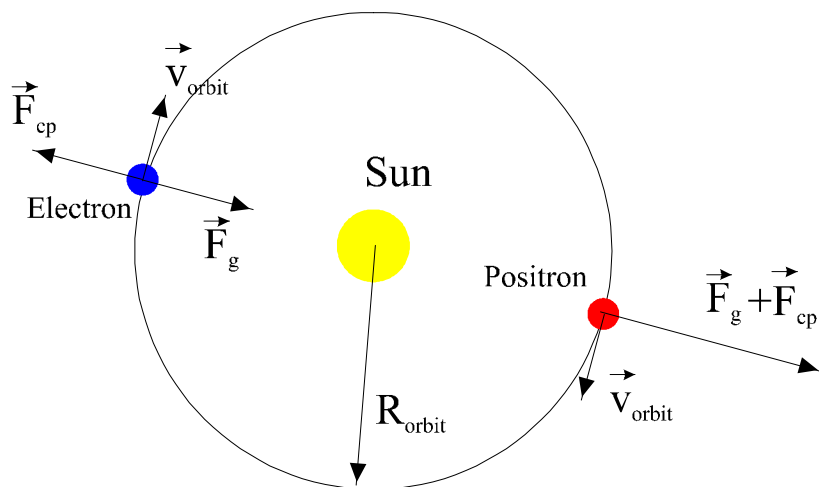


Figure F.1: Forces on electrons and positrons in orbit around the Sun as predicted by Santilli. The electrons are freely falling towards the Sun together with the Earth (not shown). The positrons are pushed away by the Sun and hence will not follow the trajectory of the electron (together with the Earth).